

# Quantum Monte Carlo studies of U(1) lattice gauge models of Kondo breakdown

Gaopei Pan<sup>1,\*</sup> and Fakher F. Assaad<sup>1,†</sup>

<sup>1</sup>*Institut für Theoretische Physik und Astrophysik and Würzburg-Dresden Cluster of Excellence ct.qmat, Universität Würzburg, 97074 Würzburg, Germany*

(Dated: December 22, 2025)

In the local-moment regime, heavy fermions are most economically described by a compact U(1) gauge theory. With this formulation of the Kondo lattice, we study a spin chain coupled to two-dimensional Dirac conduction electrons. The spin chain is described by fermionic partons carrying spin and U(1) gauge charge. The heavy-fermion quasiparticle is a bound state of a U(1) matter field carrying unit electric and U(1) gauge charge, and the fermionic parton. Using sign-problem-free determinant quantum Monte Carlo simulations, we identify two symmetry-equivalent regimes: a heavy-fermion metal with a sharp composite-fermion resonance and robust low-frequency transport, and a Kondo-breakdown metal with an incoherent resonance and vanishing low-frequency transport. For any finite lattice extent in the direction perpendicular to the chain, the Luttinger volume of the heavy-fermion phase counts both composite and conduction electrons, while in the Kondo-breakdown phase it counts only the conduction electrons. The evolution of the composite-fermion spectrum, dynamical spin structure factor, and optical conductivity provides a nonperturbative demonstration of gauge-mediated Kondo breakdown and establishes transport fingerprints of an orbital-selective Mott transition in the context of U(1) gauge theories of heavy fermions.

## Introduction—

The Kondo lattice model describes magnetic moments in a metallic environment [1, 2]. It plays an important role in a variety of domains, including heavy-fermion quantum criticality [2–5], bilayer systems of <sup>3</sup>He [6, 7], the pseudogap phase of high-temperature superconductivity [8], twisted bilayer graphene [9–13], as well as magnetic adatoms on metallic surfaces [14–17]. In this model, various phases and quantum phase transitions arise from the interplay between Kondo screening of the magnetic impurities, the magnetic Ruderman-Kittel-Kasuya-Yosida (RKKY) interaction [18–20] between magnetic moments [21], and geometric frustration [22]. The heavy-fermion phase of the Kondo lattice is a Fermi liquid with a Luttinger volume that counts both the conduction electrons and spin degrees of freedom. This defines the large Fermi surface [23–25]. As the effective mass grows, various instabilities of the heavy-fermion Fermi liquid can occur. In Hertz–Millis-type transitions, the heavy fermions in the vicinity of the large Fermi surface undergo magnetic ordering [2, 4]. Other instabilities involve the breakdown of Kondo screening and the concomitant reconstruction of the heavy-fermion Fermi surface [3, 26–32]. This Kondo-breakdown transition is the focus of this work.

More broadly, Kondo-breakdown transitions may be viewed as a special limit of an orbital-selective Mott (OSM) transition [27, 33–35], where one sector (e.g.,  $f$  moments) localizes while the remaining conduction bands stay itinerant, naturally driving a large-to-small Fermi-surface reconstruction and enabling strange-metal transport without well-defined Landau quasiparticles [3, 26, 36, 37]. This perspective is particularly transparent in dimensionally mismatched systems, in which quasi-one-dimensional spin degrees of freedom are Kondo-

coupled to higher-dimensional conduction electrons [15–17], providing a tunable setting to access orbital-selective physics and its transport consequences. Importantly, local and mesoscopic probes can directly interrogate such non-quasiparticle transport: STM can resolve the spatially inhomogeneous Kondo hybridization and its collapse near criticality [15–17], while recent shot-noise measurements in heavy-fermion nanowires reveal a strongly suppressed Fano factor that cannot be accounted for within a quasiparticle-based Fermi-liquid picture [37, 38], offering a direct window into strange-metal current carried by collective, strongly correlated excitations [39].

The pristine Kondo-breakdown transition does not involve symmetry breaking and has an odd number of impurity spins per unit cell [40]. While the heavy-fermion Fermi liquid satisfies the Luttinger theorem [24, 25], the Kondo-breakdown phase violates it [26, 41]. For dense systems, and owing to Oshikawa’s topological proof of the Luttinger theorem, this violation necessitates topological degeneracy and is referred to as the FL\* phase in which local moments and conduction decouple [23, 42]. A model amenable to negative-sign-free quantum Monte Carlo simulations that exhibits a pristine Kondo-breakdown transition consists of a spin-1/2 chain antiferromagnetically coupled to two-dimensional Dirac electrons [15]. Assume that the size of the lattice hosting the Dirac electrons perpendicular to the chain is  $L_y$  such that the unit cell hosts  $L_y$  conduction electrons and a single spin-1/2 degree of freedom. In the Kondo-breakdown phase, the Luttinger volume, corresponding to the fraction of the Brillouin-zone volume  $V_{BZ}$  enclosed by the Fermi surface, reads  $\frac{V}{V_{BZ}} = \frac{1}{2} \bmod(L_y, 2)$ , whereas in the heavy-fermion phase the spin participates in the Luttinger volume and the relation becomes  $\frac{V}{V_{BZ}} = \frac{1}{2} \bmod(L_y + 1, 2)$  [15, 23]. An understanding of this quantum phase transition in

terms of transport has remained elusive, due to the difficulty of computing the electrical current of the composite fermion particle [26, 41].

Here we introduce a minimal lattice-gauge formulation of a dimensionally mismatched Kondo lattice, motivated by a sign-problem-free setting of a spin- $\frac{1}{2}$  chain coupled to two-dimensional Dirac electrons [15]. Using determinant quantum Monte Carlo [43, 44], we identify a Kondo-coherent regime and a Kondo-breakdown regime from the composite-fermion spectrum, and we compute the optical conductivity along the chain by analytically continuing current-current correlations [45–47]. This provides controlled transport fingerprints of orbital selectivity across a pristine Kondo-breakdown transition.

*Model and numerical method.*— Our model is motivated by the fermionic parton representation of the Kondo lattice model [15, 16, 48–50]. Here, the spin 1/2 degree of freedom is expressed as:  $\hat{\mathbf{S}}_r = \frac{1}{2} \sum_{\sigma, \sigma'} \hat{f}_{r, \sigma}^\dagger \boldsymbol{\sigma}_{\sigma, \sigma'} \hat{f}_{r, \sigma'}$  with constraint,  $\sum_{\sigma} \hat{f}_{r, \sigma}^\dagger \hat{f}_{r, \sigma} = 1$ . In the above  $\boldsymbol{\sigma}$  is the vector of Pauli spin matrices. The gauge degrees of freedom correspond to the Hubbard-Strotonovich (HS) fields and the constraint endows the fermionic parton with an emergent local U(1) gauge charge [48, 51–53]. Omitting the amplitude fluctuations of the HS fields and adding dynamics in terms of electric fields, one arrives to the following lattice gauge formulation of the Kondo lattice (see supplemental material).

$$H = \sum_{\langle i, j \rangle, \sigma} t_{i, j} \hat{c}_i^\dagger \hat{c}_j + J \sum_r \left( \hat{f}_r^\dagger \hat{U}_{r, r+a_x} \hat{f}_{r+a_x} + \text{H.c.} \right) + h \sum_b \hat{E}_b^2 + h_m \sum_r \hat{e}_r^2 + V \sum_r \left( \hat{c}_r^\dagger \hat{z}_r^\dagger \hat{f}_r + \text{H.c.} \right) \quad (1)$$

Here  $[\hat{U}_b, \hat{E}_b] = \hat{U}_b$  and  $[\hat{z}_r, \hat{e}_r] = \hat{z}_r$  and we have suppressed the spin indices for clarity. Since the U(1) gauge field originate from a HS transformation they will be compact variables. The  $c$  electrons reside on a two-dimensional square lattice with  $\pi$  flux per plaquette,  $t_{ij} = \pm t$ , resulting in a Dirac semimetal with a vanishing density of states at the Fermi level. They carry spin and electric charge both being globally conserved. The  $f$ -fermions form a one-dimensional chain along the  $x$ -direction, connected by the link variables  $\hat{U}_{r, r+a_x}$ . They carry spin and locally conserved U(1) gauge charge. The matter field  $\hat{z}_r$  has unit electric and U(1) gauge charges.

A central gauge-invariant object in our analysis is the composite-fermion

$$\hat{\Psi}_r = \hat{z}_r^\dagger \hat{f}_r, \quad (2)$$

which is invariant under local U(1) gauge transformations. This operator plays a crucial role in the low-temperature heavy-fermion physics of our model: it represents a naturally emergent quasi-particle that carries electric charge and spin but no gauge charge. If the  $\hat{\Psi}_r^\dagger$

operator creates a coherent quasi-particle that participates in the Luttinger volume, the ground state corresponds to the heavy-fermion phase. This is certainly the case in the limit where  $h_m \rightarrow 0$ : the imaginary-time fluctuations of the matter field are suppressed and  $\hat{z}_r^\dagger$  can be replaced by a static phase, as in the large-N mean-field approximation (see supplemental material).

Compared to more complicated quasiparticles in the full Kondo model [50, 54, 55], the composite fermion here takes a particularly simple form. In the DQMC simulations,  $\hat{z}_r(\tau)$  is represented by a space and time dependent phase, such that including it does not introduce any additional complications for Wick's theorem. This simplicity significantly improves the numerical efficiency and the quality of the composite-fermion Green's function data. It also allows for new possibilities, namely the computation of current-current correlations of the composite fermion.

We simulate Eq. (1) using the Algorithms for Lattice Fermions (ALF) [56] implementation of sign-problem-free finite temperature DQMC [43, 57] on lattices of size  $L_x \times L_y$  for the  $c$  electrons, with an  $f$  chain of length  $L_x$  embedded along the  $x$  direction. Unless otherwise noted, we use inverse temperatures up to  $\beta = 10$  and system sizes up to  $L_x = L_y = 20$ . Imaginary-time correlation functions are analytically continued to real frequencies using the ALF [56] implementation of stochastic analytic continuation [45–47]. For simplicity, in the following we set  $t = 1$ ,  $V = 1$ , and focus on the case  $h = h_m$ , which is controlled by a single parameter that tunes the strength of gauge and matter-field fluctuations.

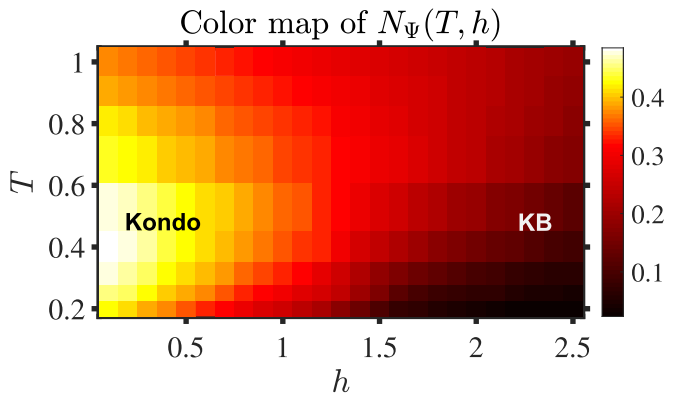


FIG. 1. Color map of the composite-fermion zero-frequency density of states  $N_\Psi(\omega = 0)$  as a function of Kondo coupling  $h$  and temperature  $T$ . Bright colors at small  $h$  indicate a Kondo-coherent phase with large  $N_\Psi$ , while dark colors at large  $h$  correspond to a Kondo breakdown (KB) phase with strongly suppressed composite quasi-particles.

### Results.—

We begin by analyzing the local composite-fermion Green's function  $G_\Psi(r, \tau) = \langle \hat{\Psi}_r(0) \hat{\Psi}_r^\dagger(\tau) \rangle$ , from which

we approximate the zero-frequency density of states as

$$N_\Psi(\omega = 0) \simeq \beta G_\Psi(r = 0, \tau = \beta/2). \quad (3)$$

Fig 1 shows a color map of  $N_\Psi(\omega = 0)$  as a function of the parameters  $h$  and temperature  $T$ . The bright phase at small  $h$  corresponds to a Kondo-coherent phase with a large composite-fermion density of states, while the dark phase at large  $h$  signals a Kondo-breakdown phase in which the composite quasiparticles are strongly suppressed. As a first approximation the data supports  $h_c \simeq 1.2$ . At low temperatures and at  $h < h_c$  we observe a depletion of spectral weight, that we attribute to finite size effects. Assuming a continuous phase transition, the correlation length in space (time) will diverge as  $\xi \simeq \left(1 - \frac{h}{h_c}\right)^{-\nu}$  ( $\xi_\tau \simeq \left(1 - \frac{h}{h_c}\right)^{-\nu z}$ ) with  $\nu$  the correlation length exponent and  $z$  the dynamical structure factor. As we approach the critical point, size effect will kick in when  $\xi \simeq L$  ( $\xi_\tau \simeq \beta$ ). In the context of local probes,  $N_\Psi(\omega = 0)$  is directly related to the local tunneling density of states accessible in STM, and to the zero-frequency limit of the shot-noise spectrum in chain-embedded geometries [37].

The composite-fermion spectral function  $A_\Psi(k, \omega)$ , where  $\langle \hat{\Psi}_k(0) \hat{\Psi}_k^\dagger(\tau) \rangle = \int_{-\infty}^{\infty} d\omega A_\Psi(k, \omega) \frac{e^{-\tau\omega}}{\pi(1+e^{-\beta\omega})}$ , provides a more direct measure of Kondo hybridization between the conduction and localized electrons. In the small- $h$  phase, Fig. 2 shows a clear hybridization and a coherent low-energy band with substantial composite-fermion weight. This feature signifies the emergence of heavy quasiparticles and corresponds to a Kondo-coherent state. As  $h$  increases, the hybridization gradually disappears, leaving behind two separate incoherent bands. The resulting spectrum indicates the destruction of the heavy quasiparticle band and the localization of the  $f$  electrons—an unambiguous signature of Kondo breakdown.

To further characterize the two phases, we compute the dynamical spin structure factor of the  $f$  chain,  $S(q, \omega)$ , shown in Fig. 3. Here  $\langle \hat{S}(q, \tau) \hat{S}(-q, 0) \rangle = \int_0^\infty d\omega S(q, \omega) \frac{e^{-\tau\omega} + e^{-(\beta-\tau)\omega}}{\pi}$ . At small  $h$ , spin excitations are broad and continuum-like, reflecting itinerant magnetic correlations mediated by the hybridized quasiparticles. In contrast, at large  $h$ , the spin spectrum develops a well-defined dispersive mode, in good agreement with that of an isolated one-dimensional Heisenberg chain. This evolution demonstrates the recovery of local-moment behavior in the Kondo-breakdown phase and corroborates the interpretation of  $f$ -electron Mott localization. We note that the the dynamics of the  $f$ -fermions at  $V = 0$  and in the limit of large values of  $h$  is described by the one-dimensional Heisenberg chain (see supplemental material).

A key observable of our study is the transport along the one-dimensional  $f$  chain. We evaluate the imaginary-time current-current correlation function

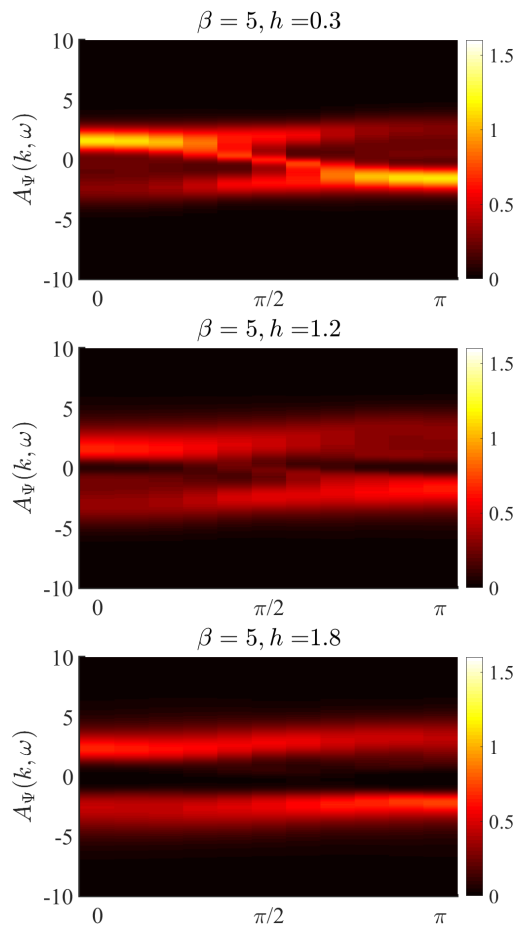


FIG. 2. Composite-fermion spectral function  $A_\Psi(k, \omega)$  at  $\beta = 5$  for three representative values of the parameters  $h$ . For small  $h$  (top panel), a clear hybridization low-energy band with substantial composite-fermion weight are visible, signalling the formation of heavy quasiparticles in the Kondo-coherent phase. Upon increasing  $h$  (middle and bottom panels), the hybridization gradually disappears and the spectrum evolves into two separated, predominantly incoherent bands, indicating the destruction of the heavy quasiparticle band and the localization of the  $f$  electrons characteristic of Kondo breakdown.

$\Lambda(\tau) = \langle J_x(\tau) J_x(0) \rangle$ , and  $J_x = \sum_r \left( i\Psi_r \Psi_{r+a_x}^\dagger + \text{h.c.} \right)$ , and obtain the optical conductivity  $\sigma'(\omega)$  along the chain by analytic continuation. The real part of the conductivity is related to  $\Lambda(\tau)$  via

$$\Lambda(\tau) = \int_0^\infty \frac{d\omega}{\pi} K(\tau, \omega) \sigma'(\omega), \quad (4)$$

with the kernel

$$K(\tau, \omega) = \omega \frac{\cosh[\omega(\tau - \beta/2)]}{\sinh(\beta\omega/2)}. \quad (5)$$

Figure 4 shows the resulting  $\sigma'(\omega)$  at fixed inverse temperature  $\beta = 5$  for several values of the transverse field  $h$ . For small  $h$  in the Kondo-coherent regime, the optical

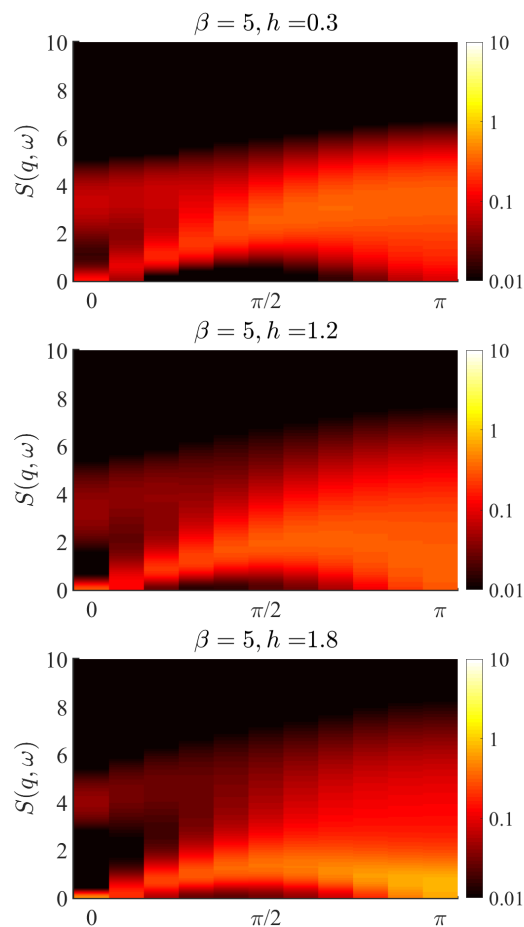


FIG. 3. Dynamical spin structure factor of the  $f$  chain,  $S_f(q, \omega)$ , at  $\beta = 5$  for three values of the parameter  $h$ . For small  $h$  (top panel), the spin response is broad and continuum-like, consistent with itinerant magnetic correlations mediated by hybridized quasiparticles in the Kondo-coherent phase. As  $h$  increases (middle and bottom panels), a well-defined dispersive mode emerges and closely follows the spectrum of an isolated one-dimensional Heisenberg chain, demonstrating the recovery of local-moment behavior and corroborating the interpretation of  $f$ -electron Mott localization in the Kondo-breakdown phase.

spectrum is dominated by a pronounced Drude-like peak at  $\omega \approx 0$ , indicating metallic transport carried by itinerant composite quasiparticles. Upon increasing  $h$  and entering the Kondo-breakdown regime, the low-frequency weight and thus the Drude component are strongly suppressed, while spectral weight is transferred to a broad hump at finite frequencies. This evolution of  $\sigma'(\omega)$  signals a metal-to-Mott-insulator transition in the  $f$  sector, whereas the Dirac  $c$  electrons remain itinerant, providing direct dynamical evidence for an orbital-selective Mott transition.

**Summary and conclusions.**— The one-dimensional spin-1/2 chain antiferromagnetically coupled to two-dimensional Dirac conduction electrons is a pristine ex-

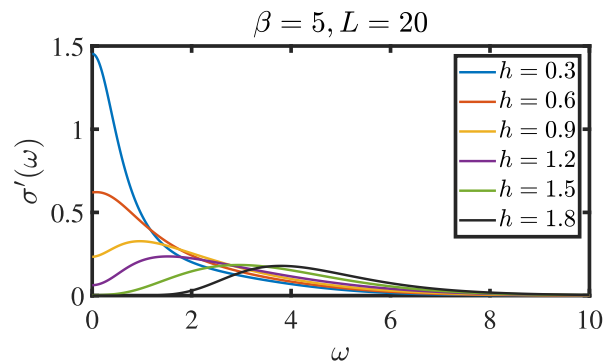


FIG. 4. Frequency dependence of the real part of the optical conductivity  $\sigma'(\omega)$  of the composite-fermion chain at inverse temperature  $\beta = 5$  for several values of the parameter  $h$ . For small  $h$ , the spectrum is dominated by a pronounced Drude-like peak at  $\omega \approx 0$ , indicating metallic transport carried by itinerant composite quasiparticles in the Kondo-coherent phase. Upon increasing  $h$ , the low-frequency weight and thus the Drude component are strongly suppressed, while spectral weight is transferred to a broad finite-frequency hump, signalling the onset of Mott-insulating behavior in the  $f$  sector. This evolution of  $\sigma'(\omega)$  with  $h$  provides dynamical evidence for an orbital-selective Mott transition, while the Dirac  $c$  electrons remain itinerant.

ample of a Kondo breakdown transition, defined by the absence of symmetry breaking between the two phases and a change of the Luttinger volume across the transition accounting for the localization of the spin degrees of freedom [15]. In this work, we introduce a minimal lattice-gauge model that captures this physics and allows us to go beyond previous DQMC studies that focused on the Kondo lattice model. In particular, the lattice-gauge formulation allows for the calculation of transport properties that capture the defining signatures of the Kondo breakdown transition. In other words, our calculations provide transport signatures of an orbital-selective Mott transition in a controlled lattice simulation.

Our approach is very similar to the Fermi-surface reconstruction without symmetry breaking introduced in Ref. [40] in the framework of a  $\mathbb{Z}_2$  gauge theory with orthogonal fermions [58, 59] and matter fields. Looking forward, our lattice-gauge formulation of the Kondo lattice opens many new avenues. It is known that lattice gauge theories can be efficiently simulated using Hybrid Monte Carlo (HMC) algorithms [60, 61], especially in the deconfined phase of compact  $U(1)$  gauge theories [62]. Achieving larger systems with the lattice-gauge formulation will allow us to study critical behavior not only of Kondo breakdown transitions, but also magnetic order-disorder transitions in dimensional mismatch Kondo lattices [16, 63, 64].

*Acknowledgment.*— The authors thank Zi Hong Liu, João C. Inácio, B. Banu and S. Biswas for discussions. GPP acknowledges the German Research Foundation (DFG) through the Würzburg-Dresden Cluster of Excel-

lence on Complexity and Topology in Quantum Matter – *ct.qmat* (EXC 2147, Project No. 390858490) as well as through the AS 120/16-2 (Project number 493886309) that is part of the collaborative research project SFB QMS funded by the Austrian Science Fund (FWF) F 86. FFA acknowledges support from the DFG under the grant DA 2805/2 (Project number 528834426). FFA and GPP gratefully acknowledge the Gauss Centre for Supercomputing e.V. ([www.gauss-centre.eu](http://www.gauss-centre.eu)) for funding this project by providing computing time on the GCS Supercomputer SUPERMUC-NG at Leibniz Supercomputing Centre ([www.lrz.de](http://www.lrz.de)), (project number pn73xu) as well as the scientific support and HPC resources provided by the Erlangen National High Performance Computing Center (NHR@FAU) of the Friedrich-Alexander-Universität Erlangen-Nürnberg (FAU) under the NHR project b133ae. NHR funding is provided by federal and Bavarian state authorities. NHR@FAU hardware is partially funded by the German Research Foundation (DFG) – 440719683. Calculations were carried out with the ALF-package [56]

- 
- \* [gaopei.pan@uni-wuerzburg.de](mailto:gaopei.pan@uni-wuerzburg.de)  
† [fakher.assaad@physik.uni-wuerzburg.de](mailto:fakher.assaad@physik.uni-wuerzburg.de)
- [1] A. C. Hewson, *The Kondo problem to heavy fermions*, 2 (Cambridge university press, 1997).
  - [2] P. Coleman, C. Pépin, Q. Si, and R. Ramazashvili, *Journal of Physics: Condensed Matter* **13**, R723 (2001).
  - [3] Q. Si, S. Rabello, K. Ingersent, and J. L. Smith, *Nature* **413**, 804 (2001).
  - [4] Q. Si and S. Paschen, *physica status solidi (b)* **250**, 425 (2013).
  - [5] F. Mazza, S. Biswas, X. Yan, A. Prokofiev, P. Steffens, Q. Si, F. F. Assaad, and S. Paschen, [arXiv:2403.12779](https://arxiv.org/abs/2403.12779) [[cond-mat.str-el](https://arxiv.org/abs/2403.12779)].
  - [6] M. Neumann, J. Nyéki, B. Cowan, and J. Saunders, *Science* **317**, 1356 (2007), <https://www.science.org/doi/pdf/10.1126/science.1143607>.
  - [7] K. S. D. Beach and F. F. Assaad, *Phys. Rev. B* **83**, 045103 (2011).
  - [8] Y.-H. Zhang and S. Sachdev, *Phys. Rev. Res.* **2**, 023172 (2020).
  - [9] Z.-D. Song and B. A. Bernevig, *Phys. Rev. Lett.* **129**, 047601 (2022).
  - [10] J. Kang, B. A. Bernevig, and O. Vafek, *Phys. Rev. Lett.* **127**, 266402 (2021).
  - [11] Y.-Z. Chou and S. Das Sarma, *Phys. Rev. Lett.* **131**, 026501 (2023).
  - [12] H. Hu, B. A. Bernevig, and A. M. Tsvelik, *Phys. Rev. Lett.* **131**, 026502 (2023).
  - [13] L. L. H. Lau and P. Coleman, *Phys. Rev. X* **15**, 021028 (2025).
  - [14] R. Toskovic, R. van den Berg, A. Spinelli, I. S. Eliens, B. van den Toorn, B. Bryant, J. S. Caux, and A. F. Otte, *Nature Physics* **12**, 656 EP (2016).
  - [15] B. Danu, M. Vojta, F. F. Assaad, and T. Grover, *Phys. Rev. Lett.* **125**, 206602 (2020).
  - [16] B. Danu, M. Vojta, T. Grover, and F. F. Assaad, *Phys. Rev. B* **106**, L161103 (2022).
  - [17] E. Li, B. Danu, Y. Liu, H. Xie, Z. Yuan, C. Li, Y. Jiang, J. W. Y. Lam, B. Z. Tang, S. Wang, *et al.*, *Journal of the American Chemical Society* (2025).
  - [18] M. A. Ruderman and C. Kittel, *Phys. Rev.* **96**, 99 (1954).
  - [19] T. Kasuya, *Progress of theoretical physics* **16**, 45 (1956).
  - [20] K. Yosida, *Phys. Rev.* **106**, 893 (1957).
  - [21] S. Doniach, *physica B+ C* **91**, 231 (1977).
  - [22] S. Burdin, D. R. Grempel, and A. Georges, *Phys. Rev. B* **66**, 045111 (2002).
  - [23] M. Oshikawa, *Phys. Rev. Lett.* **84**, 3370 (2000).
  - [24] J. M. Luttinger, *Phys. Rev.* **119**, 1153 (1960).
  - [25] J. M. Luttinger and J. C. Ward, *Phys. Rev.* **118**, 1417 (1960).
  - [26] C. Pépin, *Phys. Rev. Lett.* **98**, 206401 (2007).
  - [27] L. de' Medici, A. Georges, G. Kotliar, and S. Biermann, *Phys. Rev. Lett.* **95**, 066402 (2005).
  - [28] Y. Komijani and P. Coleman, *Phys. Rev. Lett.* **122**, 217001 (2019).
  - [29] S. Friedemann, T. Westerkamp, M. Brando, N. Oeschler, S. Wirth, P. Gegenwart, C. Krellner, C. Geibel, and F. Steglich, *Nature Physics* **5**, 465 (2009).
  - [30] S. Friedemann, N. Oeschler, S. Wirth, C. Krellner, C. Geibel, F. Steglich, S. Paschen, S. Kirchner, and Q. Si, *Proceedings of the National Academy of Sciences* **107**,

- 14547 (2010).
- [31] S. Hartmann, N. Oeschler, C. Krellner, C. Geibel, S. Paschen, and F. Steglich, *Phys. Rev. Lett.* **104**, 096401 (2010).
- [32] J. S. Hofmann, F. F. Assaad, and T. Grover, *Phys. Rev. B* **100**, 035118 (2019).
- [33] M. Vojta, *Journal of Low Temperature Physics* **161**, 203 (2010).
- [34] L. De Leo, M. Civelli, and G. Kotliar, *Phys. Rev. Lett.* **101**, 256404 (2008).
- [35] L. de' Medici, S. R. Hassan, M. Capone, and X. Dai, *Phys. Rev. Lett.* **102**, 126401 (2009).
- [36] Y. Luo, L. Pourovskii, S. Rowley, Y. Li, C. Feng, A. Georges, J. Dai, G. Cao, Z. Xu, Q. Si, *et al.*, *Nature materials* **13**, 777 (2014).
- [37] L. Chen, D. T. Lowder, E. Bakali, A. M. Andrews, W. Schrenk, M. Waas, R. Svagera, G. Eguchi, L. Prochaska, Y. Wang, *et al.*, *Science* **382**, 907 (2023).
- [38] Y. Wang, C. Setty, S. Sur, L. Chen, S. Paschen, D. Natelson, and Q. Si, *Phys. Rev. Res.* **6**, L042045 (2024).
- [39] X. Li, J. Kono, Q. Si, and S. Paschen, *Frontiers in Electronic Materials* **2**, 934691 (2023).
- [40] S. Gazit, F. F. Assaad, and S. Sachdev, *Phys. Rev. X* **10**, 041057 (2020).
- [41] I. Paul, C. Pépin, and M. R. Norman, *Phys. Rev. Lett.* **98**, 026402 (2007).
- [42] T. Senthil, S. Sachdev, and M. Vojta, *Phys. Rev. Lett.* **90**, 216403 (2003).
- [43] R. Blankenbecler, D. J. Scalapino, and R. L. Sugar, *Phys. Rev. D* **24**, 2278 (1981).
- [44] F. Assaad and H. Evertz, in *Computational Many-Particle Physics* (Springer, 2008) pp. 277–356.
- [45] A. W. Sandvik, *Phys. Rev. B* **57**, 10287 (1998).
- [46] K. Beach, arXiv preprint cond-mat/0403055 (2004).
- [47] H. Shao and A. W. Sandvik, *Physics Reports* **1003**, 1 (2023), progress on stochastic analytic continuation of quantum Monte Carlo data.
- [48] M. Raczkowski, B. Danu, and F. F. Assaad, *Phys. Rev. B* **106**, L161115 (2022).
- [49] M. Raczkowski and F. F. Assaad, *Phys. Rev. B* **109**, 205154 (2024).
- [50] B. Danu, Z. Liu, F. F. Assaad, and M. Raczkowski, *Phys. Rev. B* **104**, 155128 (2021).
- [51] N. Read and D. Newns, *Journal of Physics C: Solid State Physics* **16**, 3273 (1983).
- [52] A. Auerbach and K. Levin, *Phys. Rev. Lett.* **57**, 877 (1986).
- [53] S. Saremi and P. A. Lee, *Phys. Rev. B* **75**, 165110 (2007).
- [54] T. A. Costi, *Phys. Rev. Lett.* **85**, 1504 (2000).
- [55] M. Raczkowski and F. F. Assaad, *Phys. Rev. Lett.* **122**, 097203 (2019).
- [56] F. F. Assaad, M. Bercx, F. Goth, A. Götz, J. S. Hofmann, E. Huffman, Z. Liu, F. P. Toldin, J. S. E. Portela, and J. Schwab, *SciPost Phys. Codebases*, 1 (2025).
- [57] S. White, D. Scalapino, R. Sugar, E. Loh, J. Gubernatis, and R. Scalettar, *Phys. Rev. B* **40**, 506 (1989).
- [58] R. Nandkishore, M. A. Metlitski, and T. Senthil, *Phys. Rev. B* **86**, 045128 (2012).
- [59] M. Hohenadler and F. F. Assaad, *Phys. Rev. B* **100**, 125133 (2019).
- [60] S. Duane, A. D. Kennedy, B. J. Pendleton, and D. Roweth, *Phys. Lett.* **B195**, 216 (1987).
- [61] S. Beyl, F. Goth, and F. F. Assaad, *Phys. Rev. B* **97**, 085144 (2018).
- [62] K. Feng, C. Chen, and Z. Y. Meng, arXiv:2508.16298 (2025), arXiv:2508.16298 [cond-mat.str-el].
- [63] Z. H. Liu, B. Frank, L. Janssen, M. Vojta, and F. F. Assaad, *Phys. Rev. B* **107**, 165104 (2023).
- [64] B. Frank, Z. H. Liu, F. F. Assaad, M. Vojta, and L. Janssen, *Phys. Rev. B* **108**, L100405 (2023).
- [65] J. Villain, *Journal de Physique* **36**, 581 (1975).
- [66] W. Janke and H. Kleinert, *Nuclear Physics B* **270**, 135 (1986).
- [67] C. Wu and S.-C. Zhang, *Phys. Rev. B* **71**, 155115 (2005).

**SUPPLEMENTAL MATERIALS FOR**  
**GAUGE-MEDIATED ORBITAL-SELECTIVE MOTT TRANSITION: A QUANTUM MONTE**  
**CARLO STUDY**

**Section I. HEISENBERG LIMIT**

In the  $V = 0$  case, the Hamiltonian reduces to

$$H = J \sum_r \left( \hat{f}_r^\dagger \hat{U}_{r,r+a_x} \hat{f}_{r+a_x} + \text{H.c.} \right) + h \sum_b \hat{E}_b^2, \quad (\text{S1})$$

where  $\hat{U}_b = e^{iA_b}$  and  $\hat{E}_b = \frac{\partial}{\partial iA_b}$ . It is convenient to work in a representation where  $\hat{A}_b$  is diagonal. Omitting the bond index for notational simplicity, we write  $\hat{A}_b|\phi\rangle = \phi|\phi\rangle$  with  $\phi \in [0, 2\pi)$ , while in this representation  $\hat{E}_b = \frac{\partial}{\partial iA_b}$  has eigenstates  $|E\rangle$  defined via  $\langle\phi|E\rangle = e^{i\phi E}$  with  $E \in \mathbb{Z}$ . The corresponding resolutions of the identity read

$$\int_0^{2\pi} d\phi |\phi\rangle\langle\phi| = \frac{1}{2\pi} \sum_{E \in \mathbb{Z}} |E\rangle\langle E| = \hat{1}. \quad (\text{S2})$$

To formulate the path integral, we need the matrix element  $\langle\phi'|e^{-\Delta\tau h \hat{E}_b^2}|\phi\rangle$ . Inserting the resolution of the identity in the  $|E\rangle$  basis and using the Poisson summation formula, we obtain the Villain approximation [65, 66]

$$\langle\phi'|e^{-\Delta\tau h \hat{E}_b^2}|\phi\rangle \propto \exp \left[ -\frac{1}{2\Delta\tau h} (1 - \cos(\phi - \phi')) \right]. \quad (\text{S3})$$

In the limit  $h \rightarrow \infty$ , our model maps onto an SU(2) quantum antiferromagnet. We again start from the  $h = \infty$  limit, where the rotor degrees of freedom are frozen, and treat the hopping  $J$  in second-order degenerate perturbation theory. As mentioned above, hopping of a fermion with flavor index  $\alpha$  from site  $i$  to its nearest-neighbor site  $j$  leaves the rotor in an excited state with an energy cost of order  $h$ . The only way to remove this excitation is for a fermion with flavor index  $\alpha'$  to hop back from  $j$  to  $i$ . These virtual processes generate the effective SU(2) Heisenberg model

$$\hat{H}_{h \rightarrow \infty} \propto -\frac{J^2}{h} \sum_{\langle ij \rangle} \left( \hat{D}_{ij}^\dagger \hat{D}_{ij} + \hat{D}_{ij} \hat{D}_{ij}^\dagger \right), \quad (\text{S4})$$

with

$$\hat{D}_{ij} = \sum_{\alpha=1}^2 \hat{f}_{i\alpha}^\dagger \hat{f}_{j\alpha}. \quad (\text{S5})$$

In our simulations we work at half filling, with on average one fermion per two sites in the  $f$  chain. In this regime, the effective low-energy theory is a 1d antiferromagnetic Heisenberg chain, and we indeed observe antiferromagnetic correlations in the  $f$  sector.

**Section II. PARTITION FUNCTION AND SIGN PROBLEM FREE**

Using the Eq. (S3), the whole partition is

$$\begin{aligned} Z &= \int \left( \prod_{\tau_l=1}^{L_\tau} \prod_{x=\{r,b\}} d\phi_b(\tau_l) d\psi_r(\tau_l) \right) \left( \prod_{\tau_l} \prod_{x=\{r,b\}} e^{-\frac{1}{2\Delta\tau h} [1 - \cos(\phi_b(\tau_l) - \phi_b(\tau_l+1))]} e^{-\frac{1}{2\Delta\tau h m} [1 - \cos(\varphi_r(\tau_l) - \varphi_r(\tau_l+1))]} \right) \\ &\quad \prod_{\sigma} \text{Tr}_F \prod_{\tau_l=1}^{L_\tau} \left[ \left( \prod_{\langle i,j \rangle} e^{-\Delta\tau \hat{c}_{i,\sigma}^\dagger t_{ij} \hat{c}_{j,\sigma}} \right) \left( \prod_r e^{-\Delta\tau J \hat{f}_{r,\sigma}^\dagger e^{i\phi_b(\tau_l)} \hat{f}_{r+a_x,\sigma} + \text{h.c.}} e^{-\Delta\tau V \hat{c}_{r,\sigma}^\dagger e^{i\varphi_r(\tau_l)} \hat{f}_{r,\sigma} + \text{h.c.}} \right) \right] \\ &= \int \left( \prod_{\tau_l=1}^{L_\tau} \prod_{x=\{r,b\}} d\phi_b(\tau_l) d\psi_r(\tau_l) \right) \left( \prod_{\tau_l} \prod_{x=\{r,b\}} e^{-\frac{1}{2\Delta\tau h} [1 - \cos(\phi_b(\tau_l) - \phi_b(\tau_l+1))]} e^{-\frac{1}{2\Delta\tau h m} [1 - \cos(\varphi_r(\tau_l) - \varphi_r(\tau_l+1))]} \right) \\ &\quad \prod_{\sigma} \det \{ I + B_{L_\tau}^\sigma B_{L_\tau-1}^\sigma \cdots B_2^\sigma B_1^\sigma \} \end{aligned} \quad (\text{S6})$$

where  $B^\sigma(\tau_l)$  corresponding to  $\left(\prod_{\langle i,j \rangle} e^{-\Delta\tau \hat{c}_{i,\sigma}^\dagger t_{ij} \hat{c}_{j,\sigma}}\right) \left(\prod_r e^{-\Delta\tau J f_{r,\sigma}^\dagger e^{i\varphi_b(\tau_l)} f_{r+a_x,\sigma} + \text{h.c.}} e^{-\Delta\tau V \hat{c}_{r,\sigma}^\dagger e^{i\psi_r(\tau_l)} f_{r,\sigma} + \text{h.c.}}\right)$ , whose matrix elements are numbers (functions of the HS fields) in the single-particle basis and contain no fermionic operators.

After the following unitary particle–hole transformation  $P$ :

$$\begin{aligned} \hat{c}_{i,\downarrow} &\rightarrow (-1)^i \hat{c}_{i,\downarrow}^\dagger & \hat{c}_{i,\downarrow}^\dagger &\rightarrow (-1)^i \hat{c}_{i,\downarrow} \\ \hat{f}_{r,\downarrow} &\rightarrow (-1)^{r+1} \hat{f}_{r,\downarrow}^\dagger & \hat{f}_{r,\downarrow}^\dagger &\rightarrow (-1)^{r+1} \hat{f}_{r,\downarrow} \end{aligned} \quad (\text{S7})$$

After the unitary particle–hole transformation, which doesn't change the determinants, introduced above, the  $B$  matrix in the spin-down sector satisfy  $B_i^\downarrow = (B_i^\uparrow)^*$ , so that the corresponding fermionic determinants are complex conjugates of each other,

$$P \det\left\{I + B_{L_r}^\downarrow B_{L_r-1}^\downarrow \cdots B_2^\downarrow B_1^\downarrow\right\} P^{-1} = \left[\det\left\{I + B_{L_r}^\uparrow B_{L_r-1}^\uparrow \cdots B_2^\uparrow B_1^\uparrow\right\}\right]^*, \quad (\text{S8})$$

and the weight is a real positive number  $|\det\{I + B_{L_r}^\uparrow \cdots B_1^\uparrow\}|^2 \geq 0$ , implying the absence of a fermion sign problem [67].

### II. A. Connection with Kondo–Heisenberg model

We briefly recall how the Kondo–Heisenberg model can be rewritten as a lattice  $U(1)$  gauge theory, following Ref. [48]. We start from

$$\hat{H} = \sum_{\langle i,j \rangle, \sigma} \left(\hat{c}_i^\dagger t_{i,j} \hat{c}_j + \text{h.c.}\right) + \frac{J_k}{2} \sum_r \hat{c}_r^\dagger \boldsymbol{\sigma} \hat{c}_r \cdot \hat{\mathbf{S}}_r + J_h \sum_{\langle r,r' \rangle} \hat{\mathbf{S}}_r \cdot \hat{\mathbf{S}}_{r'}, \quad (\text{S9})$$

and represent the local moments by Abrikosov fermions

$$\hat{\mathbf{S}}_r = \frac{1}{2} \hat{f}_r^\dagger \boldsymbol{\sigma} \hat{f}_r, \quad \hat{f}_r^\dagger = (\hat{f}_{r,\uparrow}^\dagger, \hat{f}_{r,\downarrow}^\dagger), \quad (\text{S10})$$

Introducing the fermion bilinears

$$\hat{V}_r = \hat{f}_r^\dagger \hat{c}_r, \quad \hat{D}_b = \hat{f}_r^\dagger \hat{f}_{r'} \quad (b = \langle r, r' \rangle), \quad (\text{S11})$$

the Kondo and Heisenberg terms can be written as perfect squares,

$$\hat{H} = -t \sum_{\langle i,j \rangle} (\hat{c}_i^\dagger \hat{c}_j + \text{h.c.}) - \frac{J_k}{8} \sum_r [(\hat{V}_r + \hat{V}_r^\dagger)^2 + (i\hat{V}_r - i\hat{V}_r^\dagger)^2] - \frac{J_h}{8} \sum_{b=\langle r,r' \rangle} [(\hat{D}_b + \hat{D}_b^\dagger)^2 + (i\hat{D}_b - i\hat{D}_b^\dagger)^2] + \hat{H}_U. \quad (\text{S12})$$

Decoupling these squares with complex Hubbard–Stratonovich fields  $b_r$  (on sites) and  $\chi_b$  (on bonds), and taking the limit  $U \rightarrow \infty$ , the partition function can be written as a path integral

$$Z = \text{Tr} e^{-\beta \hat{H}} = \int \mathcal{D}\{f^\dagger f\} \mathcal{D}\{c^\dagger c\} \mathcal{D}\{\chi_b\} \mathcal{D}\{b_r\} \mathcal{D}\{a_0\} e^{-S}, \quad (\text{S13})$$

with an action of the form

$$\begin{aligned} S = \int_0^\beta d\tau \left\{ \frac{2}{J_h} \sum_b |\chi_b(\tau)|^2 + \frac{2}{J_k} \sum_r |b_r(\tau)|^2 + \sum_{i,j} c_i^\dagger(\tau) [\partial_\tau \delta_{ij} - T_{ij}] c_j(\tau) \right. \\ \left. + \sum_r |b_r(\tau)| \left[ e^{i\varphi_r(\tau)} f_r^\dagger(\tau) c_r(\tau) + \text{h.c.} \right] + \sum_r f_r^\dagger(\tau) [\partial_\tau - ia_{0,r}(\tau)] f_r(\tau) \right. \\ \left. + \sum_{b=\langle r,r' \rangle} |\chi_b(\tau)| \left[ f_r^\dagger(\tau) e^{-i \int_r^{r'} \mathbf{a}(\ell,\tau) \cdot d\ell} f_{r'}(\tau) + \text{h.c.} \right] \right\}, \quad (\text{S14}) \end{aligned}$$

where we have parametrized  $b_r = |b_r| e^{i\varphi_r}$  and  $\chi_b = |\chi_b| e^{i \int_r^{r'} \mathbf{a} \cdot d\ell}$ . The phases  $\varphi_r(\tau)$  and the link variables  $e^{-i \int_r^{r'} \mathbf{a} \cdot d\ell}$ , together with the temporal component  $a_{0,r}(\tau)$ , transform as a compact  $U(1)$  gauge field under  $f_r(\tau) \rightarrow e^{i\theta_r(\tau)} f_r(\tau)$ , while the conduction electrons  $c_r$  remain gauge neutral. After integrating out the fermions one obtains

$$Z = \int \mathcal{D}\{\chi_b\} \mathcal{D}\{b_r\} \mathcal{D}\{a_0\} e^{-(S_0 - \log \det M)}, \quad (\text{S15})$$

where  $S_0$  collects the purely bosonic terms and  $M$  is the fermionic matrix.

Upon freezing the amplitudes  $|b_r|$  and  $|\chi_b|$  and discretizing imaginary time[48], the remaining compact phases  $\varphi_r(\tau_l)$  and  $\int_r^{r'} \mathbf{a}(\ell, \tau_l) \cdot d\ell$  precisely correspond to the  $U(1)$  gauge link variables  $e^{i\varphi_r(\tau_l)}$  and  $e^{i\phi_b(\tau_l)}$  introduced in our lattice model in the main text.

$$\begin{aligned}
S = \int_0^\beta d\tau & \left\{ \frac{2}{J_h} \sum_b |\chi_b(\tau)|^2 + \frac{2}{J_k} \sum_r |b_r(\tau)|^2 + \sum_{i,j} \mathbf{c}_i^\dagger(\tau) [\partial_\tau \delta_{i,j} - T_{i,j}] \mathbf{c}_j(\tau) \right. \\
& + \sum_r |b_r(\tau)| \left[ e^{i\varphi_r(\tau)} \mathbf{f}_r^\dagger(\tau) \mathbf{c}_r(\tau) + h.c. \right] \\
& \left. + \sum_r \mathbf{f}_r^\dagger(\tau) [\partial_\tau - ia_{0,r}(\tau)] \mathbf{f}_r(\tau) + ia_{0,r}(\tau) + \sum_{b=\langle r,r' \rangle} |\chi_b(\tau)| \left[ \mathbf{f}_r^\dagger(\tau) e^{-i \int_r^{r'} \mathbf{a}(l,\tau) dl} \mathbf{f}_{r'}(\tau) + h.c. \right] \right\}
\end{aligned} \tag{S16}$$

At this stage, we have obtained all parts of the  $U(1)$  gauge model used in the main text, except for the dynamical term of the  $U(1)$  field.

### Section III. MEAN-FIELD FORMULATION AND KUBO FORMULA

#### III. A. Noninteracting multi-band Hamiltonian

At the mean-field level we consider an  $(L+1)$ -band tight-binding Hamiltonian

$$\begin{aligned}
H_0 &= \sum_{i,j} (t_{ij} c_i^\dagger c_j + h.c.) + J \sum_r (f_r^\dagger f_{r+\hat{x}} + h.c.) + V \sum_r (c_r^\dagger f_r + h.c.) \\
&= \sum_k \sum_{m,n=1}^{L+1} d_{k,m}^\dagger H_{mn}(k) d_{k,n} \\
&= \sum_k \sum_{n=1}^{L+1} E_n(k) \gamma_{k,n}^\dagger \gamma_{k,n}.
\end{aligned} \tag{S17}$$

Here we have defined

$$d_{k,n}^\dagger = \begin{cases} c_{k,n}^\dagger, & n = 1, \dots, L, \\ f_k^\dagger, & n = L+1, \end{cases} \tag{S18}$$

and diagonalized the single-particle Hamiltonian as  $H(k) = U(k)E(k)U^\dagger(k)$ , where  $E(k) = \text{diag}\{E_1(k), \dots, E_{L+1}(k)\}$  and  $\gamma_k^\dagger = d_k^\dagger U(k)$ . The equilibrium single-particle density matrix in this basis is

$$G_{rs}(k) = \langle d_{k,r}^\dagger d_{k,s} \rangle = \sum_n U_{rn}(k) f(E_n(k)) U_{ns}^\dagger(k), \tag{S19}$$

where  $f(E) = 1/(e^{\beta E} + 1)$  is the Fermi function.

It is convenient to introduce projection operators onto the single-particle eigenstates,

$$P_n(k) = U(k)_{:,n} U^\dagger(k)_{n,:}, \quad H(k) = \sum_n E_n(k) P_n(k), \tag{S20}$$

so that

$$G(k) = \sum_n f(E_n(k)) P_n(k), \quad e^{-itH(k)} = \sum_n e^{-itE_n(k)} P_n(k). \tag{S21}$$

For this tight-binding model, the band dispersion is obtained by diagonalizing the Bloch Hamiltonian, and the color scale represents the  $f$ -electron weight of each eigenstate,  $|U_{L+1,i}(k)|^2$ .

In the main text we focus on the bare parameters  $V = 1$  and  $J = 1$ . When the parameter  $h$  is finite but not too large, gauge fluctuations suppress the relevant mean-field amplitudes, leading to renormalized couplings  $V_{\text{eff}} < V$  and  $J_{\text{eff}} < J$ . To illustrate the corresponding band-structure evolution, Fig. S1 compares a representative choice  $(V, J) = (1.0, 1.0)$  with a reduced set  $(V, J) = (0.5, 0.5)$  (both at  $t = 1.0$ ). The reduced-parameter case closely mimics the regime discussed in the first panel of Fig. 2(a) in the main text: a pronounced hybridized band emerges, with substantial  $f$ -electron character over a broad range of momenta, reflecting strong  $c$ - $f$  mixing.

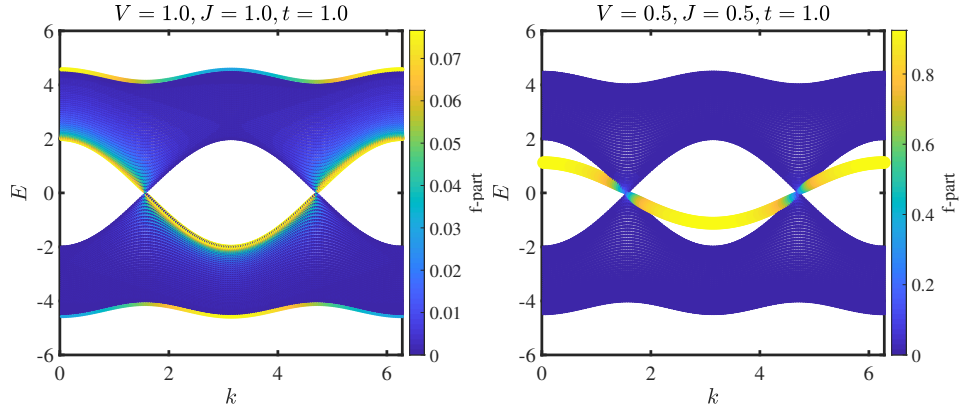


FIG. S1. Band structure of the one-dimensional tight-binding model for two sets of parameters. The dispersions are obtained by diagonalizing the Bloch Hamiltonian, and the color scale encodes the  $f$ -electron component of the  $i$ -th band at momentum  $k$ , quantified by  $|U_{L+1,i}(k)|^2$ ; brighter (yellow) points correspond to states with larger  $f$ -electron weight. Left:  $V = 1.0$ ,  $J = 1.0$ ,  $t = 1.0$ . Right:  $V = 0.5$ ,  $J = 0.5$ ,  $t = 1.0$ .

### III. B. Current operator and kinetic energy

We couple the  $f$ -fermion hopping to an external vector potential  $\mathbf{A}(t)$  via the Peierls substitution

$$H = \sum_{i,j} (t_{ij} c_i^\dagger c_j + \text{h.c.}) + J \sum_{\langle r,r' \rangle} \left( f_r^\dagger f_{r'} e^{\frac{2\pi i}{\Phi_0} \int_r^{r'} \mathbf{A}(t) \cdot d\ell} + \text{h.c.} \right) + V \sum_r (c_r^\dagger f_r + \text{h.c.}), \quad (\text{S22})$$

where  $\Phi_0$  is the flux quantum and we have in mind nearest-neighbor hopping along the  $x$  direction.

Expanding to linear order in  $\mathbf{A}(t)$  we obtain the interaction Hamiltonian

$$H_I(t) = \frac{2\pi}{\Phi_0} \hat{\mathbf{J}}_p \cdot \mathbf{A}(t), \quad (\text{S23})$$

which defines the paramagnetic current operator

$$\hat{\mathbf{J}}_p = i \sum_{i,j} (\mathbf{r}_j - \mathbf{r}_i) J_{ij} f_i^\dagger f_j. \quad (\text{S24})$$

The diamagnetic contribution is

$$\mathbf{J}_D(t) = - \sum_{i,j} (\mathbf{r}_j - \mathbf{r}_i) J_{ij} f_i^\dagger f_j [(\mathbf{r}_j - \mathbf{r}_i) \cdot \mathbf{A}(t)], \quad (\text{S25})$$

and the total physical current (per lattice length  $L$ ) reads

$$\mathbf{J}^{\text{tot}}(t) = - \frac{2\pi}{\Phi_0 L} \left[ \hat{\mathbf{J}}_p + \frac{2\pi}{\Phi_0} \mathbf{J}_D(t) \right]. \quad (\text{S26})$$

In what follows we focus on the longitudinal component and drop vector notation for brevity.

For nearest-neighbor hopping along the chain, the paramagnetic current can be written in momentum space as

$$\hat{J}_p = iJ \sum_i (f_i^\dagger f_{i+\hat{x}} - f_{i+\hat{x}}^\dagger f_i) = -2J \sum_k \sin k f_k^\dagger f_k \equiv \sum_{k,n,m} B_{nm}(k) d_{k,n}^\dagger d_{k,m}, \quad (\text{S27})$$

with

$$B_{nm}(k) = -2J \sin k \delta_{n,L+1} \delta_{m,L+1}. \quad (\text{S28})$$

Similarly, the kinetic-energy term is

$$K = \sum_{i,j} (\mathbf{r}_j - \mathbf{r}_i)^2 J_{ij} f_i^\dagger f_j = \sum_k 2J \cos k f_k^\dagger f_k \equiv \sum_{k,n,m} C_{nm}(k) d_{k,n}^\dagger d_{k,m}, \quad (\text{S29})$$

with

$$C_{nm}(k) = 2J \cos k \delta_{n,L+1} \delta_{m,L+1}. \quad (\text{S30})$$

Using Eq. (S19), its expectation value is

$$\langle K \rangle = \sum_k \text{Tr}[C(k) G(k)]. \quad (\text{S31})$$

### III. C. Current–current correlation function

We set  $\hbar = 1$  and define the retarded current–current correlation function

$$\Lambda(\omega) = i \int_0^\infty dt e^{i(\omega+i\eta)t} \langle [\hat{J}_p, \hat{J}_p^H(-t)] \rangle_0, \quad (\text{S32})$$

where the Heisenberg operator is evolved with  $H_0$  and  $\langle \dots \rangle_0$  denotes the thermal average. Writing  $\hat{J}_p$  in the  $d$ -basis and using standard Wick contractions, one obtains

$$\begin{aligned} \Lambda(\omega) &= i \int_0^\infty dt e^{i(\omega+i\eta)t} \sum_k \text{Tr} \left\{ G(k) [B(k), e^{-itH(k)} B(k) e^{itH(k)}] \right\} \\ &= i \sum_k \sum_{m,n} \int_0^\infty dt e^{i(\omega+i\eta+E_m(k)-E_n(k))t} \text{Tr} \left\{ G(k) [B(k), P_n(k) B(k) P_m(k)] \right\}. \end{aligned} \quad (\text{S33})$$

Evaluating the time integral and using  $G(k) = \sum_x f(E_x(k)) P_x(k)$  yields

$$\Lambda(\omega) = \sum_k \sum_{m,n} \frac{f(E_n(k)) - f(E_m(k))}{\omega + i\eta + E_m(k) - E_n(k)} \text{Tr} [B(k) P_n(k) B(k) P_m(k)]. \quad (\text{S34})$$

### III. D. Optical conductivity

Finally, the longitudinal optical conductivity follows from the Kubo formula

$$\sigma(\omega) = \left( \frac{2\pi}{\Phi_0} \right)^2 \frac{1}{L} \frac{1}{i(\omega + i\eta)} \left[ \langle K \rangle + \Lambda(\omega) \right], \quad (\text{S35})$$

with  $\langle K \rangle$  and  $\Lambda(\omega)$  given above. Equivalently, separating real and imaginary parts,

$$\begin{aligned} \sigma(\omega) &= \left( \frac{2\pi}{\Phi_0} \right)^2 \frac{1}{L} \frac{1}{i(\omega + i\eta)} \left[ \sum_{k,n} f(E_n(k)) \text{Tr} [C(k) P_n(k)] + \sum_{k,m,n} \frac{f(E_n(k)) - f(E_m(k))}{\omega + i\eta + E_m(k) - E_n(k)} \right. \\ &\quad \left. \times \text{Tr} [B(k) P_n(k) B(k) P_m(k)] \right] \end{aligned} \quad (\text{S36})$$

where in the last line we have used Eq. (S34) together with  $B_{nm}(k) = -2J \sin k \delta_{n,L+1} \delta_{m,L+1}$  and  $C_{nm}(k) = 2J \cos k \delta_{n,L+1} \delta_{m,L+1}$ .

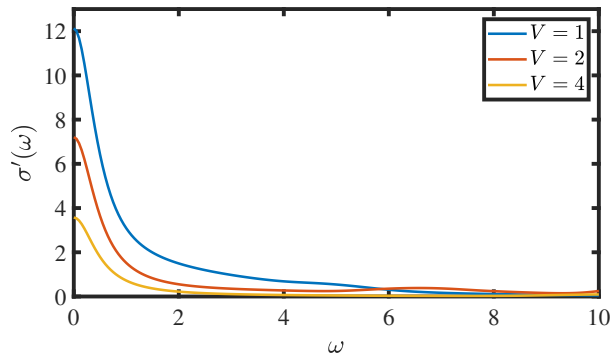


FIG. S2. For  $L = 100$ ,  $J = 0.5$ ,  $t = 1$ ,  $\beta = L$ ,  $\Delta\omega = 0.05$ , and  $\eta = 10\Delta\omega$ , the mean-field results are shown in the figure. It can be seen that when  $V$  takes moderate values, the zero-frequency conductivity remains finite, corresponding to the Kondo phase. In contrast, when  $V$  becomes too large, the hybridization band becomes overly flat, leading to a suppression of the conductivity.

## Section IV. ADDITIONAL DATA

In the main text, we presented the low-temperature optical conductivity  $\sigma'(\omega)$  of the composite-fermion chain, the composite-fermion spectral function  $A_\Psi(k, \omega)$ , and the dynamical spin structure factor of the  $f$  chain  $S_f(q, \omega)$  for three representative values of the transverse field  $h$  (see Figs. 2–4). In this Supplementary Material we extend these results in two complementary directions. First, we provide a denser scan of  $h$  at fixed low temperature (the same  $\beta = 5$  as used in the main text) in order to better resolve how the fermionic, spin, and transport responses evolve across the transition from the Kondo-coherent regime to the Kondo-breakdown regime. Second, we select three representative values of  $h$  (one in the Kondo-coherent regime, one near the transition, and one in the Kondo-breakdown regime) and present results at multiple temperatures. This temperature-dependent dataset clarifies how the Drude response, hybridization features in  $A_\Psi(k, \omega)$ , and the spin dynamics are thermally broadened and redistributed.

### IV. A. Extended low- $T$ scan in $h$ .

Figure S4 shows  $\sigma'(\omega)$  at fixed  $\beta$  for an extended set of  $h$  values. In the small- $h$  regime the spectrum is dominated by a Drude-like response near  $\omega \simeq 0$ , consistent with metallic transport of itinerant composite quasiparticles in the Kondo-coherent regime. As  $h$  increases, the low-frequency weight is progressively suppressed and spectral weight is transferred to finite frequencies, signaling the gradual loss of coherent transport and the onset of Mott-insulating behavior in the  $f$  sector. The corresponding evolution in the composite fermion spectrum and spin spectrum is also shown in Figs. S4. In particular, the coherent hybridized band in  $A_\Psi(k, \omega)$  weakens with increasing  $h$  and eventually gives way to two separated incoherent bands, while the spin response evolves toward that of an effective one-dimensional Heisenberg chain, corroborating the Kondo-breakdown interpretation discussed in the main text.

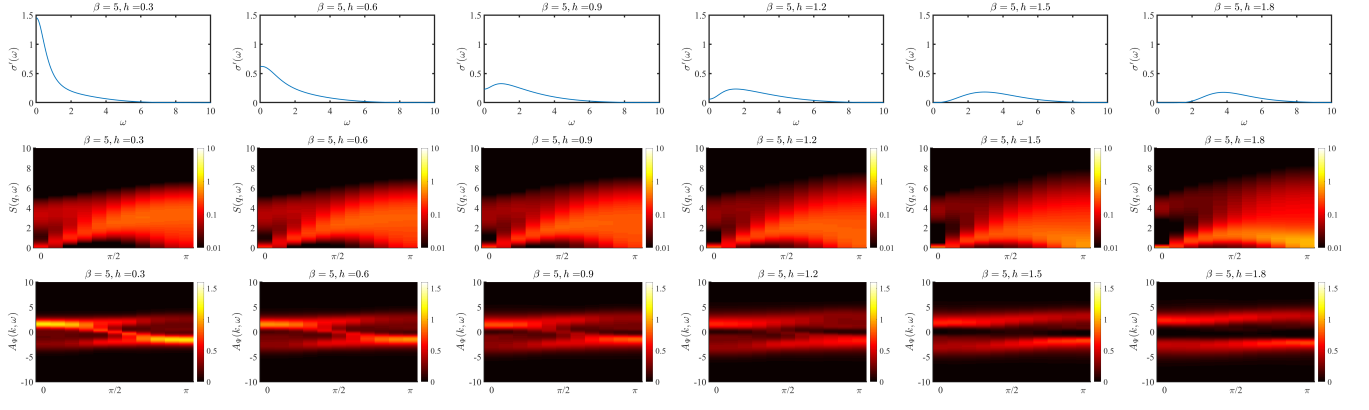


FIG. S3. **Low-temperature  $h$  scan.** Low-temperature cuts (fixed inverse temperature  $\beta = 5$ ) of three key observables as a function of  $h$ : (top row) the real part of the optical conductivity of the composite-fermion chain,  $\sigma'(\omega) \equiv \text{Re} \sigma(\omega)$ ; (middle row) the dynamical spin structure factor of the  $f$  chain,  $S_f(q, \omega)$ ; (bottom row) the composite-fermion spectral function,  $A_\Psi(k, \omega)$ . Each column corresponds to a different value of  $h$  (from left to right: increasing  $h$ ), spanning the evolution from the Kondo-coherent regime (small  $h$ ) to the Kondo-breakdown regime (large  $h$ ). In the small- $h$  regime,  $\sigma'(\omega)$  exhibits a pronounced low-frequency (Drude-like) response and  $A_\Psi(k, \omega)$  shows a coherent hybridized band, while at larger  $h$  the low-frequency optical weight is strongly suppressed, the hybridization features in  $A_\Psi(k, \omega)$  disappear, and  $S_f(q, \omega)$  evolves toward a well-defined dispersive mode consistent with local-moment dynamics.

#### IV. B. Temperature dependence at representative $h$ .

To complement the low- $T$   $h$  scan, we fix three representative values  $h$  and study the temperature evolution of  $\sigma'(\omega)$ ,  $A_\Psi(k, \omega)$ , and  $S_f(q, \omega)$  (Figs. S4–S6). These supplementary data provide a more complete view of how gauge fluctuations controlled by  $h$  and thermal fluctuations cooperate to suppress Kondo hybridization and drive orbital-selective Mott localization in the  $f$  sector.

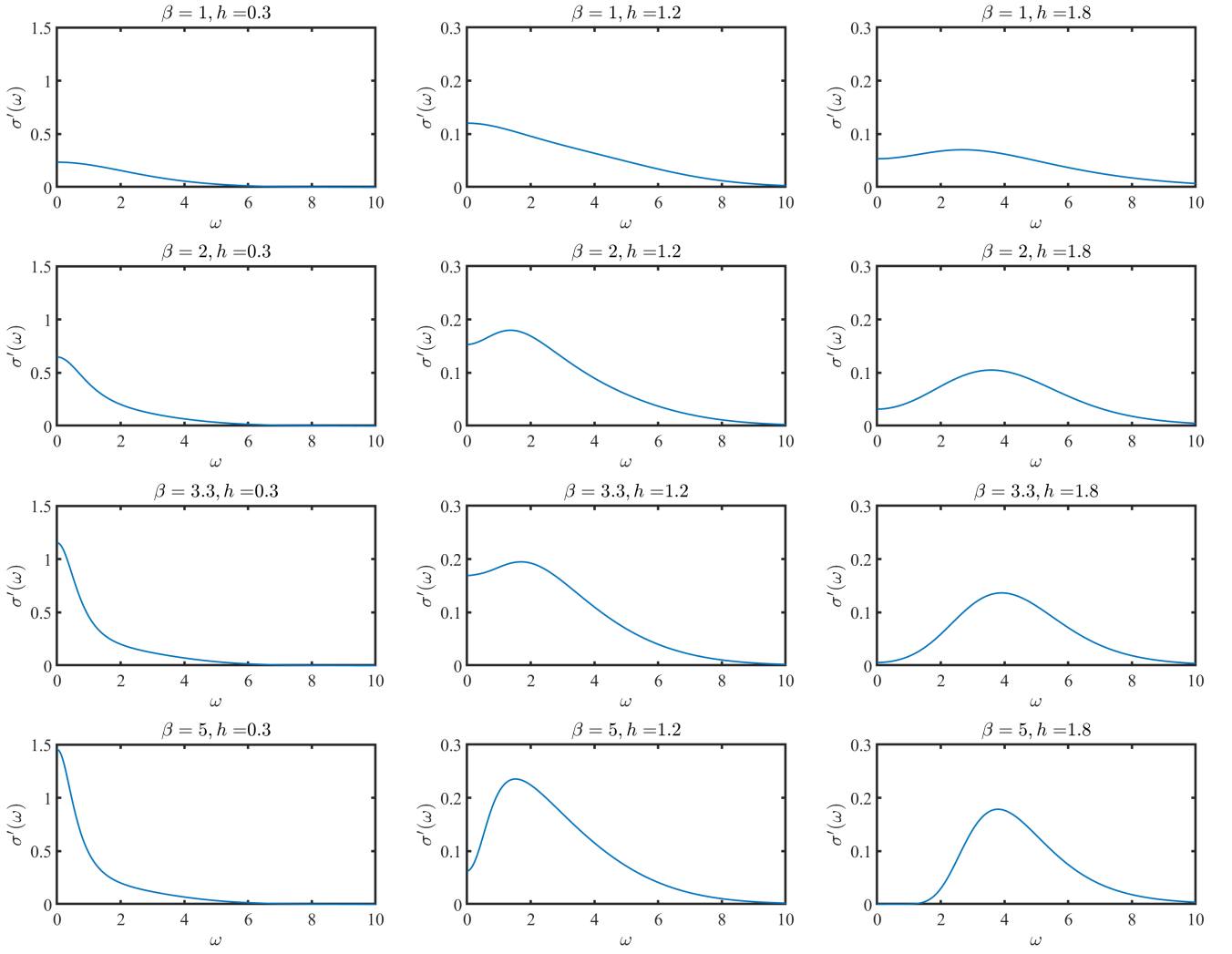


FIG. S4. **Temperature evolution of the optical conductivity at representative  $h$ .**  $\sigma'(\omega) \equiv \text{Re} \sigma(\omega)$  at three representative values  $h = 0.3, 1.2, 1.8$  for a range of inverse temperatures  $\beta = 1, 2, 3.3, 5$ .

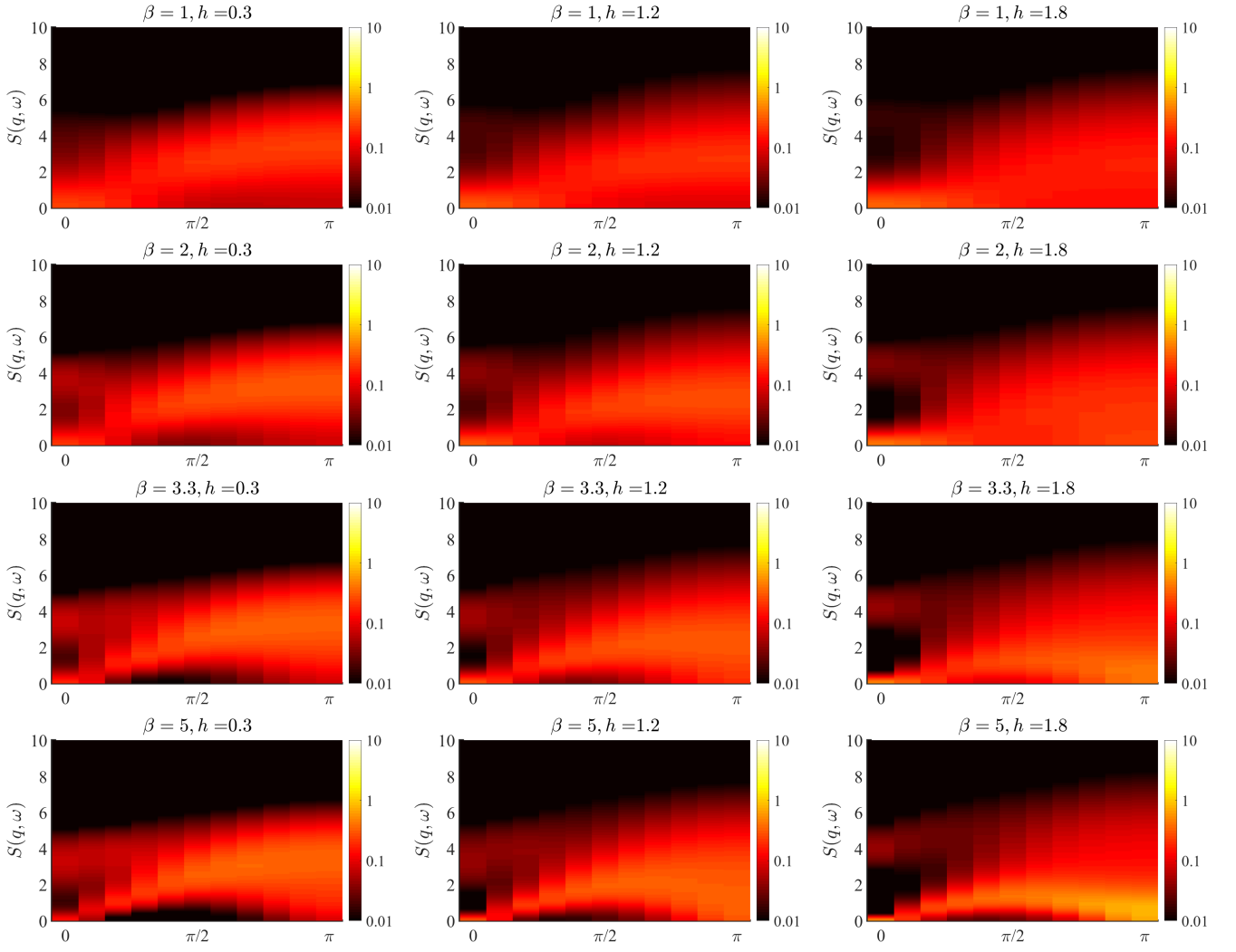


FIG. S5. **Temperature evolution of the spin dynamics at representative  $h$ .** Dynamical spin structure factor  $S_f(q, \omega)$  at different  $h$  for the same set of temperatures as in Fig. S4.

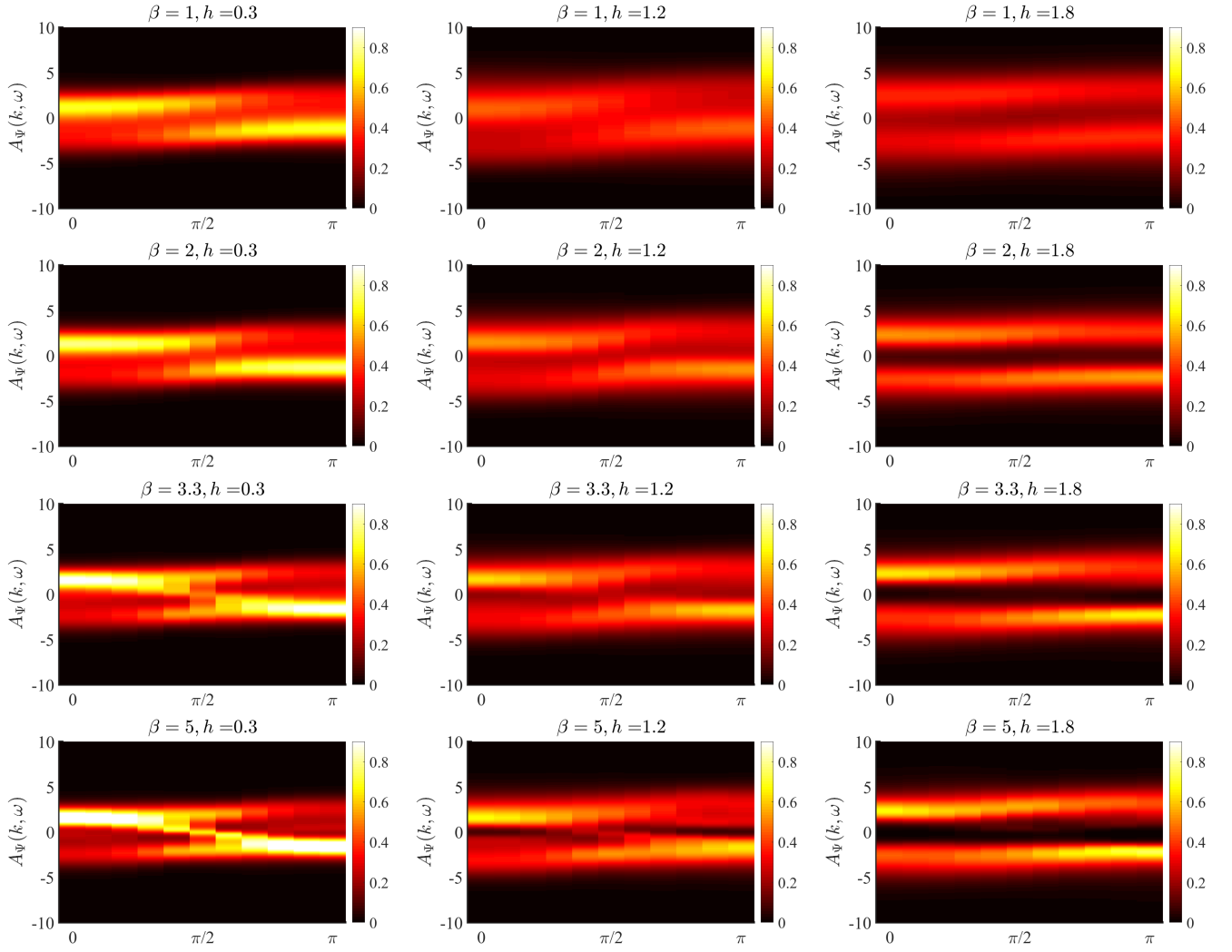


FIG. S6. Temperature evolution of the composite-fermion spectrum at representative  $h$ . Composite-fermion spectral function  $A_\Psi(k, \omega)$  at different  $h$  for the same set of temperatures as in Fig. S4.